

Fast LiDAR Informed Visual Search in Unseen Indoor Environments

Ryan Gupta¹, Kyle Morgenstein¹, Steven Ortega² and Luis Sentis¹

Abstract—This paper explores the problem of planning for visual search without prior map information. We leverage the pixel-wise environment perception problem where one is given wide Field of View 2D scan data and must perform LiDAR segmentation to contextually label points in the surroundings. These pixel classifications provide an informed prior on which to plan next best viewpoints during visual search tasks. We present LIVES: LiDAR Informed Visual Search, a method aimed at finding objects of interest in unknown indoor environments. A robust map-free classifier is trained from expert data collected using a simple cart platform equipped with a map-based classifier. An autonomous exploration planner takes the contextual data from scans and uses that prior to plan viewpoints more likely to yield detection of the search target. We propose a utility function that accounts for traditional metrics like information gain and path cost and for the contextual information. LIVES is baselined against several existing exploration methods in simulation to verify its performance. It is validated in real-world experiments with single and multiple search objects with a Spot robot in two unseen environments. Videos of experiments, implementation details and open source code can be found at <https://sites.google.com/view/lives-2024/home>.

I. INTRODUCTION

Planning and real-world execution for autonomous visual exploration are receiving significant attention from the robotics community due to their relevance in a wide range of scenarios including inspection [34], target search [1, 11], disaster response [14, 39, 4], agricultural monitoring [12], reconnaissance and surveillance [15, 19, 22]. Active planners in unknown spaces are required to make decisions based on incomplete and noisy information about partial environments. This requires planners equipped to generate high quality plans under uncertainty.

Today’s robots are frequently equipped with LiDAR sensors that cast a full view of the surroundings. State of the art exploration planners like [3, 41] demonstrate efficiency by fusing LiDAR and visual information. At the same time, the potential to use additional information from LiDAR scans for online control has grown with advances in parallel computing. While several methods exist for 3D LiDAR scan segmentation [28, 29, 44], these methods are limited by high computational requirements [16]. In contrast, real time projection-based methods often detect moving obstacles to be avoided for autonomous driving applications [10, 20, 2, 25]. Numerous planners are designed to reduce uncertainty in new environments by exploiting features common to places they

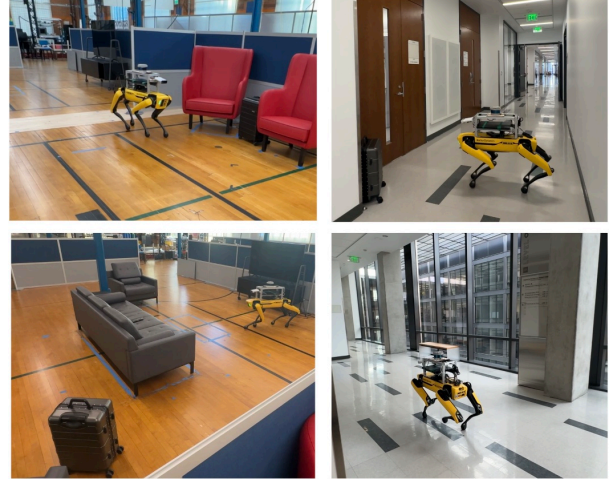


Fig. 1. LIVES allows the Spot robot to search for objects quickly in varied indoor environments. Video of experiments can be found at our website.

are designed for [32, 30]. Despite improvements in efficiency of planning algorithms for both LiDAR and vision sensors [3, 13, 35, 41], it remains an open problem to enhance performance in autonomous planning and execution for the task of visual search [42]. This work aims to reduce uncertainty in indoor environments by segmenting 2D LiDAR scans online for utilization by a next-best view (NBV) planner.

The key insight in this work is to exploit contextual information available in wide Field of View (FoV) LiDAR scans to filter out points unlikely to be the search target. This method deviates from traditional exploration methods, which focus on completeness. Rather, LIVES prioritizes regions more likely to be the search target in the robot’s surroundings. We hypothesize exploring agents can improve time efficiency in visual search by exploiting this additional information. A map based classifier is used to train a model to recognize features inherent to many indoor environments. The perception model feeds the planner the non-permanent points, *non-map points*, for use during planning. These points guide the NBV planner towards possible search target locations, assumed to be in the set of non-map points in the environment. Priority is given to features of interest using a novel utility function that accounts for both traditional metrics and non-map points. Examples of search environments are shown in Fig. 1. An overview of the proposed method can be found in Fig. 2.

The contributions of this work can be summarized as follows:

- A learning strategy for online scan segmentation as map and non-map in unseen, real-world environments
- A formulation that incorporates classified scan pixel information into a planner for visual search

¹Department of Aerospace Engineering and Engineering Mechanics, University of Texas at Austin, Austin, TX 78712 USA ryan.gupta@utexas.edu

²Department of Mechanical Engineering, University of Texas at Austin, Austin, TX 78712 USA

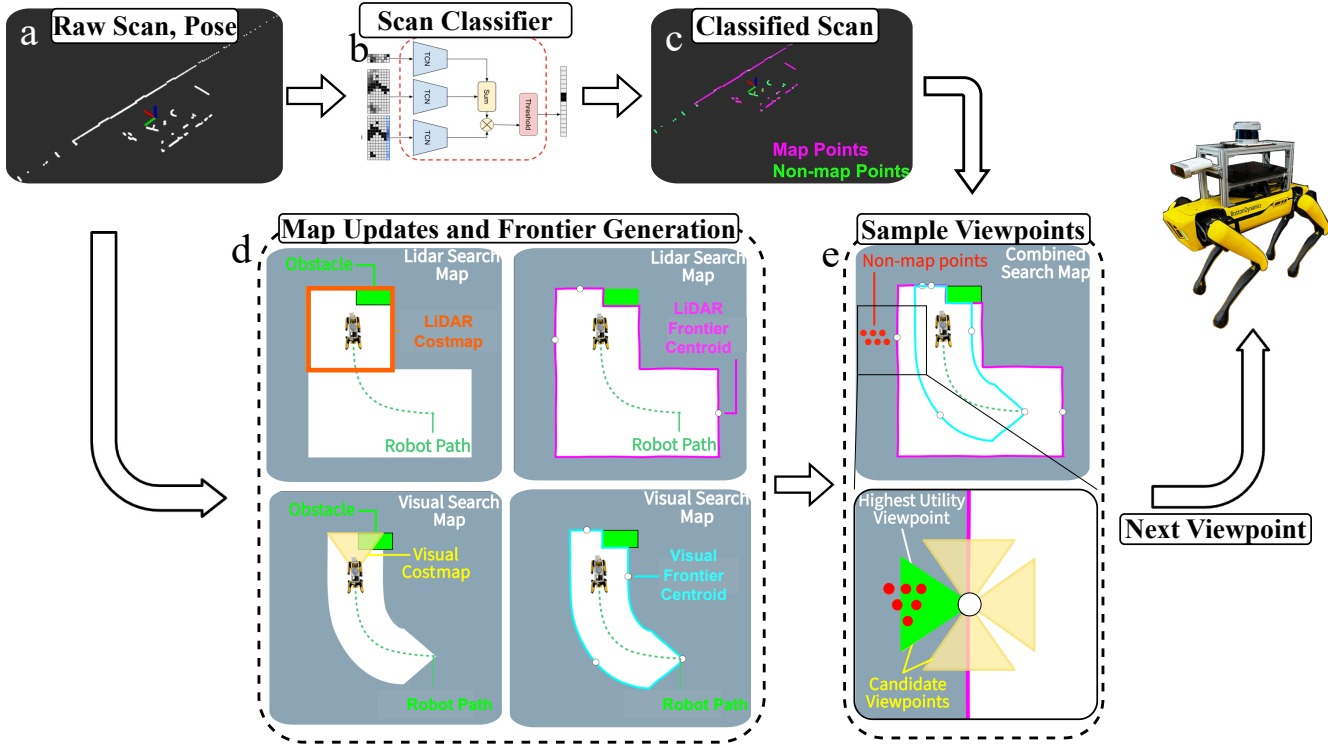


Fig. 2. Overview of a planning step of LIVES. In (a) raw 2D LiDAR scans, pose information and image data are received from the Spot robot. They are sent through a neural network classifier III-C (b) to label each point as map or non-map (c). Separately, LiDAR scans and pose data are used to maintain the global search maps for the two sensors (d). Global search maps are used to generate frontier points, shown in cyan and pink. Frontier centroids are shown as white dots and used for sampling. Each centroid has four viewpoints scored (e) III-E.2. In this toy example the left viewpoint in the lower figure in (e) will be scored highest and selected as the next waypoint due to the high number of unknown cells and non-map points observed. Finally, the selected viewpoint is sent back to the robot for execution.

- Demonstrate reduced mission completion time in the visual search task over existing planners

II. RELATED WORKS

A. Next-Best View and Multisensor Planning

Exploration is often solved using next-best viewpoint planners like Frontier Exploration [43, 13]. A common approach uses an active perception formulation to maximize entropy reduction [18, 9]. Ref. [11] combine frontier and sampling based methods while other methods leverage learning to plan [8, 21]. These methods demonstrate efficient exploration in simulation and on hardware, however none are explicitly designed for visual search using contextual information. Ref. [45] propose a POMDP for local object search in cluttered 3D environments and extend it with a 2D planner for larger areas, however, their work is aimed at 3D search for small objects, rather than quickly searching large areas.

Multisensor exploration includes LiDAR information in planning for visual exploration tasks. State of the art multisensor exploration with multiple UAVs [3] leverages the single agent exploration algorithm presented in [41]. These methods combine frontier generation for both sensors and use a single utility function to score frontier candidates for surface mapping. Ref. [26] maintains a dense 3D pointcloud for recognizing of objects in subterranean tunnel environments, which are used by a Pan-Tilt-Zoom camera. These works demonstrate efficiency in a number of real world environments, however none of these methods is designed for the environments considered in this article.

B. World Prediction Based Planning

World prediction methods typically learn a model of relevant environments and exploit their structure to explore high-value regions first. Ref. [32] use topological features from a database of tunnel networks to inform a frontier-based exploration policy. Similarly, ref. [35] use a prediction module to detect semantic objects and classify frontiers, resulting in exploring rooms first before continuing global exploration. The proposed method instead aims to ignore low value regions in order to reduce search completion time. Prediction guide the robot towards likely exit locations.

C. LiDAR Classification

Indoor 3D pointcloud classification is tackled in [36] with KPConv [37]. This requires the offline annotation and map building at instantiation and is used for simulated localization and navigation [38]. The proposed work instead focus on low computation 2D scan pixel classification. Ref. [27] presents an in depth comparison and framework for Iterative Closest Point (ICP) methods, similar to that of [36], focused on map building. Finally, [33] present a map-free framework for segmenting 3D pointclouds into ground, edges and planar points for mapping outdoor environments.

III. METHODS

The overall scan classifier and planning module are described in Fig. 2 and Alg. 1. The key components are detailed in this section.

Algorithm 1 Map-Free LiDAR Informed Search()

Input: s_i, x_i

LiDAR Scan, Robot Pose

Output: x_{next}^* (Next viewpoint) $s_i^{\text{class}} = \text{NeuralNetworkClassifier}(s_i)$ $\mathcal{M}_i^{\text{LiDAR}} \leftarrow \text{LiDARMapUpdate}(s_i, x_i, \mathcal{M}_{i-1}^{\text{LiDAR}})$ $\mathcal{M}_i^{\text{Visual}} \leftarrow \text{VisualMapUpdate}(s_i, x_i, \mathcal{M}_{i-1}^{\text{Visual}})$ $\{\mathbb{C}^{\text{LiDAR}}\} = \text{GetLiDARFrontiers}(\mathcal{M}_i^{\text{LiDAR}})$ $\{\mathbb{C}^{\text{Visual}}\} = \text{GetVisualFrontiers}(\mathcal{M}_i^{\text{Visual}})$ **for** $n \leftarrow 1$ to N **do** \triangleright for each frontier c_n in \mathbb{C} \triangleright for each viewpoint at c_n \triangleright for each viewpoint at c_n \triangleright for each viewpoint at c_n \triangleright for each viewpoint at c_n \triangleright for each viewpoint at c_n \triangleright for each viewpoint at c_n \triangleright for each viewpoint at c_n

A. Environment

The environment is described as a discrete set of points \mathcal{E} . This can be split into two subsets $\mathcal{E}^{\text{free}} \subset \mathcal{E}$ and $\mathcal{E}^{\text{occ}} \subset \mathcal{E}$, which represent the free and occupied cells in the environment. Both of these sets are initially unknown to the robot, but are assumed to follow a structure inherent in indoor environments (e.g. hallways, planar walls, open rooms and loops).

B. Ground Truth LiDAR Scan Classification

The search target of interest belongs to $\mathcal{E}^{\text{occ}} \subset \mathcal{E}$. In particular, scan classification attempts to divide \mathcal{E}^{occ} into two subsets, namely $\mathcal{E}^{\text{non-map}}$ and \mathcal{E}^{map} . In this work, \mathcal{E}^{map} are points in the environment that are deemed to be Long-Term Features (LTFs) during classification, while $\mathcal{E}^{\text{non-map}}$ are points that are either Short-Term Features (STFs) or Dynamic Features (DFs) [7]. LTFs represent the static map obstacles, STFs represent static un-mapped obstacles and DFs represent moving points. Given map information, scan points can be classified into these three categories as follows.

Let x_i denote the pose of the robot, and s_i denote observation at time step t_i . Each observation s_i consists of n_i 2D points, $s_i = \{p_i^j\}_{j=1:n_i}$. Observations are transformed from robot local frame into the global frame using an affine transformation $T_i \in SE(3)$. Finally, let map \mathcal{M} be represented as a set of lines $\{l_i\}_{1:n}$.

1) *LTF*: First, an analytic ray cast is performed [6] to determine expected laserscan based on map \mathcal{M} and current robot position x_i . Given observations, the probability that points correspond to one of the lines of that static map can be written

$$P(p_i^j | x_i, \mathcal{M}) = \exp \left(- \frac{\text{dist}(T_i p_i^j, l_j)^2}{\Sigma_s} \right) \quad (1)$$

where Σ_s is the scalar variance of observations, which comes from sensor accuracy. If Eq. 1 is greater than a threshold, point p_i^j is classified as a LTF.

2) *STF*: Remaining points will be classified as STF or DF. Observations at current time i , p_i^j , are compared with prior observations at time k , p_k^l to determine correspondence between points in subsequent observations. The likelihood of the remaining points corresponding to the same point as in a previous laserscan is computed as

$$P(p_i^j, p_k^l | x_i, x_k) = \exp \left(- \frac{\|T_i p_i^j - T_k p_k^l\|^2}{\Sigma_s} \right) \quad (2)$$

where p_k^l is the nearest point from p_i^j among points which does not belong to LTF at other timesteps, defined as

$$p_k^l = \arg \min \|T_i p_i^j - T_k p_k^l\| \quad (3)$$

When Eq. 2 is greater than some threshold, point p_i^j is classified as an STF. Remaining points in p_i^j are classified as DFs. The result is classified scan s_i^{class} .

C. Map-free LiDAR Scan Classification

The classification method defined in III-B is limited by the necessity of static map information \mathcal{M} . Therefore, this work uses supervised learning to train a model to reproduce classifications for $\{p_i^j\}_{j=1:n_i}$ in scan s_i .

1) *Dataset and Data Acquisition*: The dataset \mathcal{D} consists of tuples of data from the ground truth classification model. The tuples are given as $\mathcal{D} = \{(x_i, s_i, s_i^{\text{class}})\}_{i=1}^N$, where x_i represents robot pose, s_i is the raw LiDAR scan data, and s_i^{class} is the classified scan. N is the total number of data points collected. Data acquisition with a robot requires a human expert to control, which is difficult to scale due to mechanical limits of the robot. To ease data acquisition we design a steerable cart platform (see website for details) to mimic the robot. Human operators easily maneuver this cart to obtain the dataset. We mount a Velodyne Puck LiDAR for recording scan information and a front-mounted Intel RealSense T265 stereo camera to obtain the cart's odometry estimate, required for running the ground-truth classification. A laptop maintains the pose estimate [7] and collects the data. The Puck has $n_i = 897$ and classified scans are recorded at 5Hz. A dataset of size $N \simeq 145,000$ is collected in this study, representing roughly 8 hours of time. In practice, the model only receives raw scan data, pose estimate and previously predicted labels from the robot during operation and must classify pixel-wise the scan online. Training data can be found on the project website.

2) *Architecture and Training*: We formulate pixel-wise LiDAR classification as a supervised learning problem during training and an auto-regressive problem during inference. Given dataset \mathcal{D} , we shuffle and batch the dataset between time steps and locations to minimize location-based and temporal bias during training. Because no map information is provided explicitly, we provide the model with a history buffer of k time steps for scan ranges and robot poses, and $k - 1$ previously estimated ground truth labels. Because we do not have access to ground truth labels at inference time, we corrupt the ground truth labels during training by randomly bit-flipping the classification of 10%

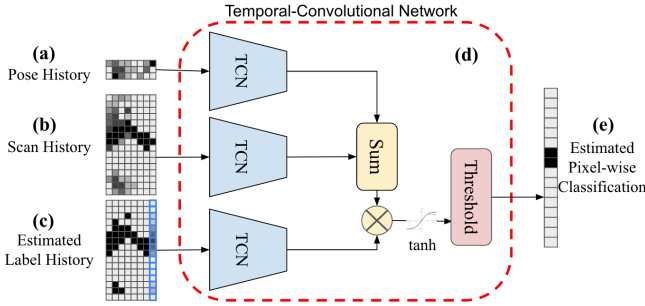


Fig. 3. Pixel-wise LiDAR scan classification model architecture. This model enables speeding up search by providing contextual information to the planner. k is the length of the history buffer. (a) $[3, k]$ pose history matrix containing $[x, y, \theta]$. (b) $[n_i, k]$ LiDAR range history matrix. (c) $[n_i, k - 1] \cup [n_i, 1]$ estimated label history matrix concatenated with its pixel-wise exponential weighted average. (d) The model consists of three temporal-convolutional encoders (TCN), one for each input. The encoded poses, scans, and labels are combined to produce a pixel-wise classification of the LiDAR scan. In (e) a threshold (positive/negative) is applied to the raw logits such that each pixel is classified as either a map point or a non-map point.

of the labels, chosen by sampling indices from a uniform random distribution. We then take the exponential weighted average of the last $k - 1$ corrupted pixel-wise classifications to estimate the current pixel-wise classification. This estimate is concatenated with the $k - 1$ corrupted ground truth labels to produce a k -length matrix of estimated scan labels. During inference, the label history buffer is populated by previous estimates from the policy. The history buffer is concatenated with the updated pixel-wise exponential weighted average. At initialization, the policy is bootstrapped with zero-value poses, scans, and labels, and run for k steps of inference until the history buffer is full. Code for training a model can be found on the project website.

The full model architecture is shown in Fig. 3. The policy consists of a temporal-convolutional encoder (TCN) for each input. Each encoder contains a single convolutional layer with scan-wise circular padding and a single linear layer. The scan and label encoders have kernel size $[k, k]$, and the pose encoder has kernel size $[1, 3]$. Hyperbolic tangent activations are used for all layers. The output of each encoder is the same size as the LiDAR scan to be classified. The output of the pose encoder is summed with the output of the scan encoder as a pose correction, and then normalized by applying a hyperbolic tangent function. The resulting LiDAR scan encoding is multiplied element-wise with the label encoding. A threshold (positive/negative) is applied to the raw logits such that each pixel is classified as either a map point or a non-map point. The policy is trained with mean squared error loss against ground truth classifications. Training for 20 epochs on a workstation Nvidia 3080 12Gb takes 3 minutes.

D. Map Updates

Two global occupancy maps (search maps) are maintained. One for the LiDAR and the other for the visual sensor. Global search maps are implemented using ROS Costmap2D [23]. All cells in both global maps are initialized to be unknown, $e = -1 \forall e \in \mathcal{E}$. The robot is equipped with a visual sensor with a cone shaped FoV, implemented as a triangular costmap. The LiDAR sensor has a 360 degree FoV, represented as a square-type costmap. Observations

for both sensors are a set of range estimates to the nearest occupied point $e \in \mathcal{E}^{\text{occ}}$. Points between the robot and the nearest occupied point along each ray of the LiDAR scan are free points $e \in \mathcal{E}^{\text{free}}$. Given incoming observations from the robot, each global costmap is updated as free space $e = 0$ or occupied $e = 1$. This process is shown in Fig. 2(d).

E. Multisensor Frontier Exploration

The planning module seeks to generate a viewpoint at each planning step that results in the highest likelihood to find the target of interest. This is achieved in several steps: candidate viewpoints are generated, viewpoints are scored, and finally the point with the highest score is fed to the robot for navigation to that point.

1) *Candidate Viewpoint Generation*: Frontier points in each of the two global search maps are generated using a process similar to [43], shown in Fig. 2(e). Any free cell ($e = 0$) adjacent to an unknown cell ($e = -1$) is a frontier edge, which are grouped together into frontiers. Any group of frontier points beyond a minimum size becomes its own frontier. Frontier centroids of each frontier in both the visual and LiDAR search maps are found by clustering. Four candidate viewpoints are evaluated at each frontier centroid to account for the limited FoV of the vision sensor.

2) *Viewpoint Selection*: Candidate viewpoints are selected based on a computationally efficient heuristic utility function. High value viewpoints are those that are near the robot, allow inspection of many unknown map points and result in inspection of non-map points. This process is shown in Fig. 2(f). The utility functions is a weighted sum of the following: (1) Penalize distance from robot position to viewpoint, (2) Reward expected number of unknown cells discovered, (3) Reward viewpoints with frontiers near the path to the candidate viewpoint, and (4) Reward viewpoints that result in inspection of a scaled number non-map points. Scaling parameters on each term are tuned during experiments. Weight are set such that the agent is inclined to prioritize non-map points and those viewpoints that result in high number of expected cells discovered. The next waypoint is selected by sending the highest utility viewpoint, x_{next}^* , to the robot.

IV. RESULTS

We test three hypotheses through our evaluation: (1) The proposed approach to inform an exploring agent with non-map features is effective at finding search targets, (2) LIVES reduces detection time compared against existing exploration algorithms, and (3) The proposed method can be deployed successfully on a real robot in unseen indoor environments.

A. LiDAR Scan Classification

We compare the learned classification policy to the ground truth classifier. The output of the policy is a vector of size n_i normalized between -1 and 1 for each scan point. If a value is non-negative, the point belongs to \mathcal{E}^{map} . Otherwise the point belongs to $\mathcal{E}^{\text{non-map}}$. We express performance in terms of per-scan accuracy of the classified LiDAR scans from the policy vs. ground truth from map information.

Map Name	Target Difficulty	NBVP [5]	RRT [40]	Multisensor Frontier Exploration [41]	Ground Truth Classification	LIVES (Our Method)
Apartment	Easy	112(70%)	72(80%)	36 (100%)	34(100%)	34(100%)
	Hard	177(30%)	128(60%)	106 (100%)	92(100%)	90(100%)
Office	Easy	70(80%)	54 ± (80%)	34 (100%)	26(100%)	24(100%)
	Hard	300(0%)	111 (80%)	141(90%)	99(100%)	105(100%)

TABLE I

AVERAGE TIME (S) FOR EACH METHOD TO FIND THE OBJECT OF INTEREST IN THE GIVEN SIMULATION ENVIRONMENTS.

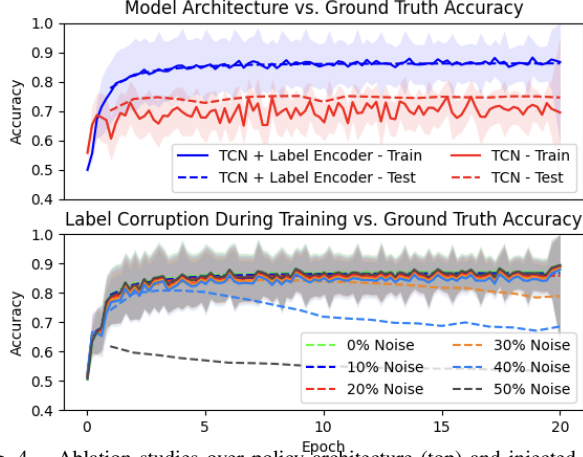


Fig. 4. Ablation studies over policy architecture (top) and injected noise during training (bottom). The inclusion of the label history buffer yields 11.63% higher test accuracy. The policy is robust up to 30% to bit-flipping errors in the label history buffer. The mean accuracy depicts the 5-step moving average.

This metric for classified scan s_i^{class} at time i compared to ground truth $s_i^{\text{class, true}}$ is given by

$$\text{accuracy} = \frac{1}{n_i} \sum_{j=0}^{n_i} \{+1 \text{ if } p_i^j == p_i^{j, \text{true}} \text{ else } 0\} \quad (4)$$

The final test accuracy of the policy compared to ground truth is $86.19\% \pm 0.03\%$ with no a priori map requirement. We perform two ablation studies, modulating the model architecture and injected noise during training, with results in Fig. 4. The inclusion of the label encoder is responsible for a 11.63% increase in test accuracy. Because the robot moves relatively slowly compared to the policy update frequency, recently predicted labels strongly bias the current estimate toward the correct classification. We fix the history buffer to 9 time steps, corresponding to 1.8 seconds. The history buffer enables the policy to reason about its environment even though no reference map is provided. During training, uniform random noise is injected into the label history buffer to simulate inference-time auto-regressive accumulated errors. The policy is robust up to 30% of injected noise before the policy begins to over-fit and performance degrades. We select a policy trained with 10% injected noise to deploy on the robot. All ablation studies were performed with a fixed seed (0) and initialized with identical weights. We do not tune the random seed.

B. Simulation and Baseline Comparison

Simulations are performed in Gazebo with the Turtlebot [31]. Move base is used to navigate to the given viewpoints [24]. Baselines are: 1) a modified Multisensor Frontier Exploration [41], 2) the Next-Best View Planner (NBVP) [5], 3) a Rapidly-Exploring Random Tree (RRT) [40], and 4)

LIVES given ground-truth scan classifications. We make the following modifications to ref. [41] for our environments. The method is projected into 2D and viewpoints are sampled *at* centroids instead of *surrounding* them. This modified multisensor frontier method is equivalent to the proposed approach without segmented scan information. Two Gazebo worlds are tested with easy and hard setups in each. A figure depicting them is shown on the project website. The first map is the apartment (20x30m) and examines the impact of non-target objects on LIVES. The easy setting has fewer objects in the environment while hard has more objects. The second map is the office (25x45m) and tests the method in a large environment under significantly varied target position. Easy and hard settings are defined by the search object in the same or different half of the environment as the robot starting position. Both difficulty levels in each map are repeated 10 times. Average detection times and success rates are reported in Table I. The time limit given to planners is 2 and 3 minutes in the apartment easy and hard settings then 3 and 5 minutes in the office easy and hard settings. Trials where the planner fails or the time limit is reached are reported as a failure and failed trials are reported as the maximum allotted time.

Results indicate that LIVES, the Ground-Truth variant and the Multisensor Frontier Exploration method significantly outperform the RRT and NBVP baselines in all settings except for the hard office setting, where the RRT method performs similarly to LIVES and Ground-Truth methods. In the easy apartment setting we observe similar performance among the three planners. In the hard setting LIVES and Ground-Truth perform nearly identically and show a 15% improvement with the addition of non-map points compared with the Multisensor method. There exists a large gap in the easy office setting with a near 30% improvement using contextual LiDAR information over the Multisensor variant. In the hard office setting, LIVES and Ground-Truth variant outperform the RRT method by 5-12%. The results indicate that LIVES outperforms the baselines across the full spectrum of environments. We hypothesize this is due to the requirement for the exploration planners to exhaustively explore the environment, whereas the proposed method focuses on non-map points, allowing the agent to move on when the target is unlikely to be nearby. These results support hypotheses (1) and (2) that contextual LiDAR information significantly improves performance in the search task.

C. Hardware Experiments

Experiments are in a 20mx30m apartment and a 15mx38m hallway environment. These two environments are not included in dataset \mathcal{D} used to train the pixel-wise classification policy. A Boston Dynamics Spot is equipped

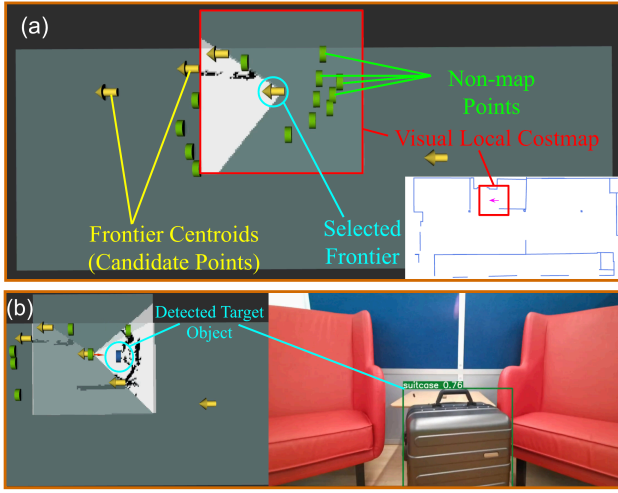


Fig. 5. A time lapse of a simple scenario. The ground truth map (20x30m) is shown in the lower right corner (a). This is unavailable to the robot and not included in the training dataset. In (a), the global search map, frontier points and non-map points are also shown. The target object is behind the robot starting position. The result of the first planning step is also shown. The planner takes advantage of the concentration of non-map points behind the robot. Figure (b) demonstrates the moment of detection and localization of the target object (suitcase).

with a Velodyne Puck LiDAR and Azure Kinect RGB-D camera. The search object is one or two small rolling suitcases. YOLOv5 [17] is used for detection. Objects are localized by first converting PointCloud data into the optical frame and then converting to pixel coordinates using camera intrinsics. Bounding boxes are then used to obtain the depth information from coinciding pixels. A time lapse of a simple trials in the apartment is shown in Fig. 5. The search target is situated behind the robot starting position. This example demonstrates the benefit of non-map information. In (b), if selecting simply based on number of unknown cells discovered, the agent may select another frontier, for example the candidate on the left hand side. However, equipped with this contextual information the agent selects the frontier that enables inspection of many non-map features nearby, resulting in detection. We compare the accuracy of the trained classifier in these out of distribution environments to ground truth information. The evaluated accuracy in the two out of distribution experimental environments are 84.0168% in the apartment over a 105 second deployment and 84.869% in the hallway over a 230 second deployment. These results demonstrate the robustness of the model in unseen environments, suggesting the model successfully identifies features common to many indoor environments. The success of LIVES onboard a real robot verify hypothesis (3). Videos of experiments, code and implementation details can be found on the project website <https://sites.google.com/view/lives-2024/home>. The video demonstrates three trials. The first and second take place in the apartment with one and two search objects, respectively. In both apartment scenarios, the robot tends to look towards furniture like couches, shelves and tables. Similarly, Spot also tends to inspect trash cans and other objects in the hallway. This behavior demonstrates the impact of non-map points and suggests the efficacy of the

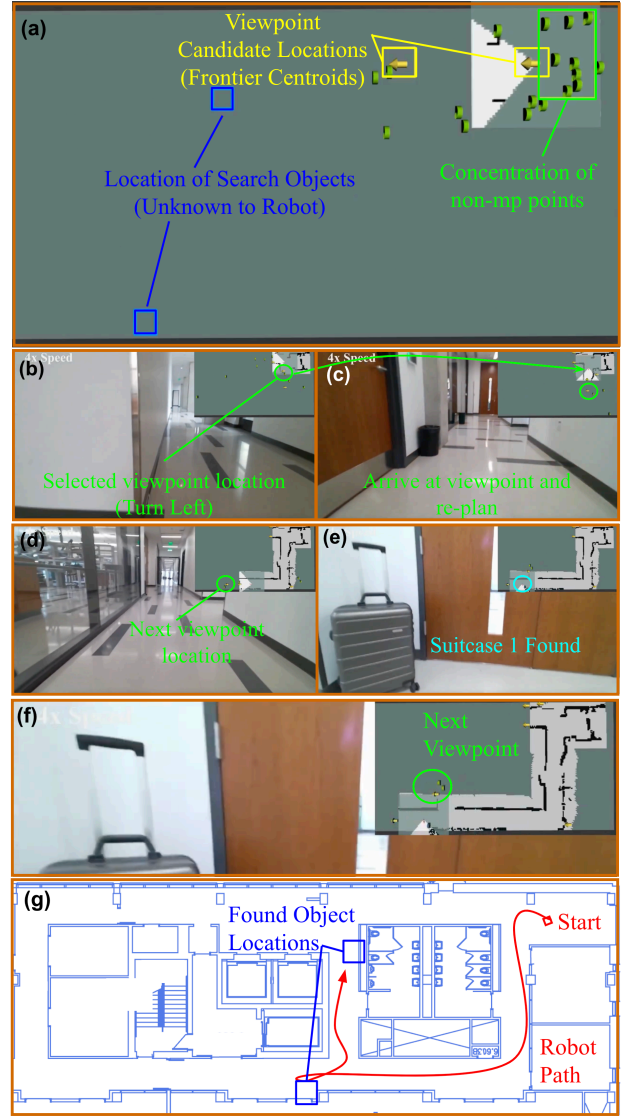


Fig. 6. A time lapse of the hallway environment (15x38m) experiment scenario. In the lower right corner of (a) is the ground truth map with the suitcase locations and non-map points near the robot shown. This information is not in the training dataset and not given to the robot. In (a) the robot pose is centered on the visual costmap. The first pose selected inspects the non-map points behind the robot. In (b) the robot chooses to turn left at the hallway split, recognizing a trash can as a non-map point. This correspondence can be seen between the non-map point in (b) appearing in the viewpoint visited by the robot in (c). In (d) the robot selects the circled viewpoint, facing to the left. This results in viewpoint (e), inspecting the suitcase, which was recognized as a non-map points in (d). In (f) the robot has just localized the first suitcase and takes the decision to return to the fork for non-map points found by that candidate viewpoint, leading to the second suitcase. (g) shows the overall robot path overlaid on the ground truth map.

segmentation policy. Several key moments in the hallway search scenario are shown in the time lapse in Fig. 6.

V. CONCLUSIONS

We introduce LIVES, a method to leverage contextual information for search in unseen environments. It is shown to outperform baselines by 10-30% in simulation. Through ablative studies, we validate our architecture and training approach for map-free scan classification. Our experiments confirm the effectiveness of the visual search planner and learning method in real-world scenarios. Ongoing work plans to expand to multi-robot applications.

VI. ACKNOWLEDGMENTS

This research was supported in part by NSF Award #2219236 (GCR: Community Embedded Robotics: Understanding Sociotechnical Interactions with Long-term Autonomous Deployments) and Living and Working with Robots, a core research project of Good Systems, a UT Grand Challenge. Any opinions, findings, and conclusions or recommendations expressed in this material are those of the author and do not necessarily reflect the views of the National Science Foundation.

REFERENCES

- [1] Haris Balta, Janusz Bedkowski, Shashank Govindaraj, Karol Majek, Pawel Musialik, Daniel Serrano, Kostas Alexis, Roland Siegwart, and Geert De Cubber. “Integrated data management for a fleet of search-and-rescue robots”. In: *Journal of Field Robotics* 34.3 (2017), pp. 539–582.
- [2] Stefan Andreas Baur, David Josef Emmerichs, Frank Moosmann, Peter Pinggera, Björn Ommer, and Andreas Geiger. “Slim: Self-supervised lidar scene flow and motion segmentation”. In: *Proceedings of the IEEE/CVF International Conference on Computer Vision*. 2021, pp. 13126–13136.
- [3] Graeme Best, Rohit Garg, John Keller, Geoffrey A Hollinger, and Sebastian Scherer. “Resilient multi-sensor exploration of multifarious environments with a team of aerial robots”. In: *Robotics: Science and Systems (RSS)*. 2022.
- [4] Qingchen Bi, Xuebo Zhang, Jian Wen, Zhangchao Pan, Shiyong Zhang, Runhua Wang, and Jing Yuan. “CURE: A Hierarchical Framework for Multi-Robot Autonomous Exploration Inspired by Centroids of Unknown Regions”. In: *IEEE Transactions on Automation Science and Engineering* 99 (2023), pp. 1–14.
- [5] Andreas Bircher, Mina Kamel, Kostas Alexis, Helen Oleynikova, and Roland Siegwart. “Receding horizon” next-best-view” planner for 3D exploration”. In: *2016 IEEE International Conference on Robotics and Automation (ICRA)*. IEEE. 2016, pp. 1462–1468.
- [6] Joydeep Biswas and Manuela Veloso. “Depth camera based indoor mobile robot localization and navigation”. In: *2012 IEEE International Conference on Robotics and Automation*. IEEE. 2012, pp. 1697–1702.
- [7] Joydeep Biswas and Manuela M Veloso. “Episodic non-markov localization”. In: *Robotics and Autonomous Systems* 87 (2017), pp. 162–176.
- [8] Yuhong Cao, Tianxiang Hou, Yizhuo Wang, Xian Yi, and Guillaume Sartoretti. “Ariadne: A reinforcement learning approach using attention-based deep networks for exploration”. In: *arXiv preprint arXiv:2301.11575* (2023).
- [9] Benjamin Charrow, Sikang Liu, Vijay Kumar, and Nathan Michael. “Information-theoretic mapping using cauchy-schwarz quadratic mutual information”. In: *2015 IEEE International Conference on Robotics and Automation (ICRA)*. IEEE. 2015, pp. 4791–4798.
- [10] Xieyuanli Chen, Benedikt Mersch, Lucas Nunes, Rodrigo Marcuzzi, Ignacio Vizzo, Jens Behley, and Cyrill Stachniss. “Automatic labeling to generate training data for on-line LiDAR-based moving object segmentation”. In: *IEEE Robotics and Automation Letters* 7.3 (2022), pp. 6107–6114.
- [11] Xuning Chen, Jianying Zheng, and Qinglei Hu. “A Hybrid Planning Method for 3D Autonomous Exploration in Unknown Environments With a UAV”. In: *IEEE Transactions on Automation Science and Engineering* (2023).
- [12] Martin Peter Christiansen, Morten Stigaard Laursen, Rasmus Nyholm Jørgensen, Søren Skovsen, and René Gislum. “Designing and testing a UAV mapping system for agricultural field surveying”. In: *Sensors* 17.12 (2017), p. 2703.
- [13] Anna Dai, Sotiris Papatheodorou, Nils Funk, Dimos Tzoumanikas, and Stefan Leutenegger. “Fast frontier-based information-driven autonomous exploration with an mav”. In: *2020 IEEE international conference on robotics and automation (ICRA)*. IEEE. 2020, pp. 9570–9576.
- [14] Jeffrey Delmerico, Elias Mueggler, Julia Nitsch, and Davide Scaramuzza. “Active autonomous aerial exploration for ground robot path planning”. In: *IEEE Robotics and Automation Letters* 2.2 (2017), pp. 664–671.
- [15] Ben Grocholsky, James Keller, Vijay Kumar, and George Pappas. “Cooperative air and ground surveillance”. In: *IEEE Robotics & Automation Magazine* 13.3 (2006), pp. 16–25.
- [16] Alok Jhaldiyal and Navendu Chaudhary. “Semantic segmentation of 3D LiDAR data using deep learning: a review of projection-based methods”. In: *Applied Intelligence* 53.6 (2023), pp. 6844–6855.
- [17] Glenn Jocher. *YOLOv5 by Ultralytics*. Version 7.0. May 2020. DOI: 10.5281/zenodo.3908559. URL: <https://github.com/ultralytics/yolov5>.
- [18] Brian J Julian, Sertac Karaman, and Daniela Rus. “On mutual information-based control of range sensing robots for mapping applications”. In: *The International Journal of Robotics Research* 33.10 (2014), pp. 1375–1392.
- [19] Li Liang, Fang Deng, Jianan Wang, Maobin Lu, and Jie Chen. “A reconnaissance penetration game with territorial-constrained defender”. In: *IEEE Transactions on Automatic Control* 67.11 (2022), pp. 6295–6302.
- [20] Minghua Liu, Yin Zhou, Charles R Qi, Boqing Gong, Hao Su, and Dragomir Anguelov. “Less: Label-efficient semantic segmentation for lidar point clouds”. In: *European Conference on Computer Vision*. Springer. 2022, pp. 70–89.
- [21] Max Lodel, Bruno Brito, Alvaro Serra-Gómez, Laura Ferranti, Robert Babuška, and Javier Alonso-Mora. “Where to look next: Learning viewpoint recommendations for informative trajectory planning”. In: *2022 International Conference on Robotics and Automation (ICRA)*. IEEE. 2022, pp. 4466–4472.
- [22] Parikshit Maini, Pratap Tokekar, and PB Sujit. “Visibility-based persistent monitoring of piecewise linear features on a terrain using multiple aerial and ground robots”. In: *IEEE Transactions on Automation Science and Engineering* 18.4 (2020), pp. 1692–1704.
- [23] Eitan Marder-Eppstein, David V. Lu, and Dave Hershberger. 2024. URL: http://wiki.ros.org/costmap_2d.
- [24] Eitan Marder-Eppstein, David V. Lu, and Dave Hershberger. 2024. URL: <https://github.com/ros-planning/navigation>.
- [25] Benedikt Mersch, Xieyuanli Chen, Ignacio Vizzo, Lucas Nunes, Jens Behley, and Cyrill Stachniss. “Receding moving object segmentation in 3d lidar data using sparse 4d convolutions”. In: *IEEE Robotics and Automation Letters* 7.3 (2022), pp. 7503–7510.
- [26] Manthan Patel, Gabriel Waibel, Shehryar Khattak, and Marco Hutter. “LiDAR-guided object search and detection in Subterranean Environments”. In: *2022 IEEE International Symposium on Safety, Security, and Rescue Robotics (SSRR)*. IEEE. 2022, pp. 41–46.
- [27] François Pomerleau, Francis Colas, Roland Siegwart, and Stéphane Magnenat. “Comparing ICP variants on real-world data sets: Open-source library and experimental protocol”. In: *Autonomous robots* 34 (2013), pp. 133–148.
- [28] Charles R Qi, Hao Su, Kaichun Mo, and Leonidas J Guibas. “Pointnet: Deep learning on point sets for 3d classification and segmentation”. In: *Proceedings of the IEEE conference*

- on computer vision and pattern recognition. 2017, pp. 652–660.
- [29] Charles Ruizhongtai Qi, Li Yi, Hao Su, and Leonidas J Guibas. “Pointnet++: Deep hierarchical feature learning on point sets in a metric space”. In: *Advances in neural information processing systems* 30 (2017).
 - [30] Santhosh K Ramakrishnan, Ziad Al-Halah, and Kristen Grauman. “Occupancy anticipation for efficient exploration and navigation”. In: *Computer Vision–ECCV 2020: 16th European Conference, Glasgow, UK, August 23–28, 2020, Proceedings, Part V* 16. Springer. 2020, pp. 400–418.
 - [31] ROBOTIS. 2024. URL: <https://www.turtlebot.com/turtlebot3/>.
 - [32] Manish Saroya, Graeme Best, and Geoffrey A Hollinger. “Online exploration of tunnel networks leveraging topological CNN-based world predictions”. In: *2020 IEEE/RSJ International Conference on Intelligent Robots and Systems (IROS)*. IEEE. 2020, pp. 6038–6045.
 - [33] Tixiao Shan and Brendan Englot. “Lego-loam: Lightweight and ground-optimized lidar odometry and mapping on variable terrain”. In: *2018 IEEE/RSJ International Conference on Intelligent Robots and Systems (IROS)*. IEEE. 2018, pp. 4758–4765.
 - [34] Chee Sheng Tan, Rosmiwati Mohd-Mokhtar, and Mohd Rizal Arshad. “A comprehensive review of coverage path planning in robotics using classical and heuristic algorithms”. In: *IEEE Access* (2021).
 - [35] Yuezhao Tao, Yuwei Wu, Beiming Li, Fernando Cladera, Alex Zhou, Dinesh Thakur, and Vijay Kumar. “SEER: Safe Efficient Exploration for Aerial Robots using Learning to Predict Information Gain”. In: *2023 IEEE International Conference on Robotics and Automation (ICRA)*. IEEE. 2023, pp. 1235–1241.
 - [36] Hugues Thomas, Ben Agro, Mona Gridseth, Jian Zhang, and Timothy D Barfoot. “Self-supervised learning of lidar segmentation for autonomous indoor navigation”. In: *2021 IEEE International Conference on Robotics and Automation (ICRA)*. IEEE. 2021, pp. 14047–14053.
 - [37] Hugues Thomas, Charles R Qi, Jean-Emmanuel Deschaud, Beatriz Marcotequi, François Goulette, and Leonidas J Guibas. “Kpconv: Flexible and deformable convolution for point clouds”. In: *Proceedings of the IEEE/CVF international conference on computer vision*. 2019, pp. 6411–6420.
 - [38] Hugues Thomas, Matthieu Gallet de Saint Aurin, Jian Zhang, and Timothy D Barfoot. “Learning Spatiotemporal Occupancy Grid Maps for Lifelong Navigation in Dynamic Scenes”. In: *2022 International Conference on Robotics and Automation (ICRA)*. IEEE. 2022, pp. 484–490.
 - [39] Teodor Tomic, Korbinian Schmid, Philipp Lutz, Andreas Domel, Michael Kassecker, Elmar Mair, Iris Lynne Grix, Felix Ruess, Michael Suppa, and Darius Burschka. “Toward a fully autonomous UAV: Research platform for indoor and outdoor urban search and rescue”. In: *IEEE robotics & automation magazine* 19.3 (2012), pp. 46–56.
 - [40] Hassan Umari. 2024. URL: https://github.com/hasauino/rrt_exploration.
 - [41] Eduard Vidal, Narcís Palomeras, Klemen Istenič, Nuno Gracias, and Marc Carreras. “Multisensor online 3D view planning for autonomous underwater exploration”. In: *Journal of Field Robotics* 37.6 (2020), pp. 1123–1147.
 - [42] Chaoqun Wang, Wenzheng Chi, Yuxiang Sun, and Max Q-H Meng. “Autonomous robotic exploration by incremental road map construction”. In: *IEEE Transactions on Automation Science and Engineering* 16.4 (2019), pp. 1720–1731.
 - [43] Brian Yamauchi. “A frontier-based approach for autonomous exploration”. In: *Proceedings 1997 IEEE International Symposium on Computational Intelligence in Robotics and Automation CIRA’97. Towards New Computational Principles for Robotics and Automation*. IEEE. 1997, pp. 146–151.
 - [44] Maciej Zamorski, Maciej Zieba, Piotr Klukowski, Rafal Nowak, Karol Kurach, Wojciech Stokowiec, and Tomasz Trzciński. “Adversarial autoencoders for compact representations of 3D point clouds”. In: *Computer Vision and Image Understanding* 193 (2020), p. 102921.
 - [45] Kaiyu Zheng, Anirudha Paul, and Stefanie Tellex. “A System for Generalized 3D Multi-Object Search”. In: *arXiv preprint arXiv:2303.03178* (2023).